Visible imaging of edge fluctuations in the TFTR tokamak

S. J. Zweben and S. S. Medley
Princeton University, Plasma Physics Laboratory, Princeton, New Jersey 08543

(Received 14 March 1989; accepted 8 June 1989)

Images of the visible light emission from the inner wall region of the TFTR tokamak [M. G. Bell *et al.*, in *Plasma Physics and Controlled Nuclear Fusion Research 1988*, Proceedings of the 12th International Conference, Nice, France (IAEA, Vienna, in press)] have been made using a rapidly gated, intensified TV camera. Strong "filamentation" of the neutral deuterium D_α light is observed when the camera gating time is $< 100\ \mu$sec during neutral-beam-heated discharges. These turbulent filaments vary in position randomly versus time and have a poloidal wavelength of $\approx$3–5 cm, which is much shorter than their parallel wavelength of ≈ 100 cm. A second and new type of edge fluctuation phenomenon, which is called a "merfe," is also described. Merfes are a regular poloidal pattern of toroidally symmetric, small-scale marfes that move away from the inner midplane during the current decay after neutral beam injection. Some tentative interpretations of these two phenomena are presented.

I. INTRODUCTION

In this paper we describe measurements of the two-dimensional (2-D) structure of fluctuations in the visible light emission observed near the inner (small major radius) wall region of TFTR.[1] Most of these measurements were made with a gated, intensified video camera viewing from the outer midplane with the TFTR periscope system.

Two different phenomena are described. The first is a rapidly time-varying and apparently turbulent "filamentation" observed in the neutral D_α emission during neutral beam injection (NBI). This filamentation, which is similar to that observed previously in Ohmic diverted plasmas on ASDEX and DITE,[2] is most likely caused by strong fluctuations of the density in the edge region.[3] If so, then several new features of this turbulence are brought out by these measurements; namely, a large fluctuation level at the inner (good curvature) region of the tokamak, a relatively large poloidal scale length compared to an ion gyroradius ($k_{\rm pol}\rho_s \approx 0.02$), and a relatively short parallel scale length compared to the toroidal circumference ($\lambda_\parallel \approx 0.1qR$).

The second phenomenon, which we call "merfes," seems to be similar to previously observed marfes.[4,5] These merfes are a poloidally regular pattern of small-scale, toroidally symmetric emitting bands that are stationary during NBI but which move slowly away from the inner equator during the plasma current decay.

II. INSTRUMENTATION

The plasma is viewed from the outer equatorial plane using the TFTR plasma TV periscope system,[6] which allows the camera to be located in the shielded basement below the tokamak. This periscope views the plasma with $f/8$ optics, and has a remote controlled field of view, focus, iris, filter, and magnification. At its highest magnification (5° field of view) the periscope has a spatial resolution of a few millimeters over about a 30×30 cm area at the tokamak inner wall.

The camera used for most of these measurements was a gated microchannel-plate-intensified, solid-state CID camera.[7] The rated sensitivity was $< 10^{-5}$ fc ($\approx 10^{-11}$ W/cm^2 at 500 nm) with a standard S-20 photocathode response. The internal microchannel plate was triggered such that each field could be exposed for a time anywhere from 1 μsec to ≈ 16 msec, while still maintaining the normal video format of 60 fields/sec. In practice, an exposure time of $\approx$10–40 μsec was used for imaging the turbulent fluctuations, while an exposure time of up to 16 msec/field was used for the slow-moving merfes.

An optical interference filter with a passband of 10 nm centered at 656 nm was used for the D_α measurements. This filter passes mainly deuterium D_α light (TFTR has $< 10\%$ of the hydrogen isotope), but is also sensitive to a nearby carbon II doublet at 658.3 nm, particularly at low density (during NBI the D_α is larger than the carbon line). The camera output was linear with respect to light intensity, and an internal automatic gain control varied the sensitivity of the microchannel plate as a whole versus time to avoid saturation. This D_α line is often monitored with discrete photodiodes,[8] but with relatively low space and time resolution.

The images were stored on a VCR in the "field" mode, i.e., without interlacing successive 16 msec fields into a normal video frame. The resulting fields had 388 pixels $\times$ 240 lines. The images were later digitized using a PC-based frame grabber and standard image processing software.

III. INTERPRETATION OF VISIBLE LIGHT EMISSION

A. General theory

In general, the light emission from a given line is given by[9]

$$I(\nu) = (\text{const}) n_e n_i \langle \sigma v \rangle, \tag{1}$$

where $I(\nu)$ is the light intensity at frequency ν, n_e is the local electron density, n_i is the local density of the relevent ion, and $\langle \sigma v \rangle$ is the excitation rate for the spectral line of that ion. Most low-Z spectral lines in tokamaks come from excited ions that exist only in a particular temperature range and so are emitted from relatively narrow toroidal shells. The pres-

 0899-8221/89/102058-08$01.90

ent periscope view will generally integrate over both the inner (small major radius) and outer (large major radius) parts of this toroidal shell.

With the neutral deuterium D_α line the ion density n_i in (1) is replaced by the neutral deuterium density n_d. The excitation rate $\langle \sigma v \rangle$ of the D_α emitting state (per atom) is a weak function of electron temperature, which peaks at about $T_e \approx 50$–100 eV, but is relatively constant over the range 10–1000 eV.[9] However, since the ionization of hydrogen is almost complete above ≈ 100 eV, these shells of D_α are located very near the plasma boundary of hot tokamaks, where $T_e = 100$ eV occurs just a few centimeters inside the last closed magnetic flux surface.[8,10]

Numerical simulation and spectroscopic observation of D_α emission for TFTR has shown[8] that this shell has a typical radial extent of about 5–10 cm radially inside the toroidally shaped "bumper limiter" that forms the inner (small major radius) wall of TFTR. Since the plasma radius is 80 cm while the inner wall radius is 99 cm, the fraction of this D_α emitting region that is inside the outermost closed flux surface varies with poloidal angle. Typically, at 30° above the inner equator the distance between the wall and the outermost flux surface is only ≈ 3 cm, so there most of this D_α emission occurs "inside" the plasma. Note that the CII lines (which constitute a possible background to the D_α light passed by this filter) form similar shells a few centimeters radially inside those of D_α. Note also that the visible light emission from the large major radius side is negligible, since the dominant neutral deuterium source was due to localized recycling at the area of plasma–surface contact along the inner bumper limiter.

According to Eq. (1), fluctuations in the local D_α emission can, in principle, be caused by variations in local values of the electron density, the neutral density, or the electron temperature. Spatial averaging will also reduce the measured intensity fluctuations, $\tilde{I}$, when the radial wavelength of the fluctuations is smaller than the radial thickness of the emitting shell. Given these various possibilities, it becomes difficult, in general, to interpret observed D_α fluctuations quantitatively in terms of local plasma density or temperature fluctuations.

However, a simplified interpretation can be made by noting that the emitted light fluctuations $\tilde{I}$ always respond linearly to electron density fluctuations $\tilde{n}_e$, whereas $\tilde{I}$ is insensitive to temperature fluctuations at the temperature of maximum emission. Thus the local D_α light fluctuations are *a priori* more likely to be caused by $\tilde{n}_e$ than $\tilde{T}_e$ (see Sec. III B for experimental tests of this).

The local neutral density n_d might also fluctuate due to a variation of the ionization fraction dependent on T_e, or to a variation in the local neutral hydrogen recycling rate dependent on the local n_e or T_e. Although it is difficult to exclude *a priori* such an influence of $\tilde{n}_d$ on the observed $\tilde{I}$, it is fairly clear that any $\tilde{n}_d$ is caused by the local $\tilde{n}_e$ and/or $\tilde{T}_e$, and would not fluctuate independently. In this case $\tilde{I}$ would be a nonlinear function of $\tilde{n}_e$ and/or $\tilde{T}_e$.

Another interpretation needs to be made concerning the extent to which the light intensity can follow rapid changes in n_e or T_e. For typical TFTR edge plasmas with $n_e \approx 10^{13}$ cm^{-3} and $T_e \approx 50$ eV the excitation rates to the $n = 3$ level of hydrogen and the deexcitation rates from $n = 3$ to $n = 2$ are typically $\approx 10^8$ sec^{-1} (Refs. 9 and 11) implying that $\tilde{I}$ will follow fluctuations with periods larger than 1 μsec, which is the range of interest for the present experiments. Over this excitation/de-excitation time a neutral hydrogen atom with an energy of a few electron-volts moves < 1 cm, and therefore is effectively representing the local $\tilde{I}$.

In summary, fluctuations in D_α light $\tilde{I}$ are most likely correlated with $\tilde{n}_e$ fluctuations, although a quantitative interpretation of $\tilde{I}$ cannot yet be made without independent knowledge of the local radial profiles of density and temperature and of the possible D_α source variations.

B. Previous experiments in tokamaks

High-speed (7000 frames/sec) movie camera pictures of ASDEX and DITE[2] showed a strong turbulent filamentation of the D_α light in Ohmic divertor discharges that is similar to that described below. In those machines, the D_α source was produced by gas puffing at either the inner or outer wall. A similar filamentation was also observed with methane or impurity injection, suggesting that the filaments were simply illuminated by the presence of emitting atoms.

An experiment to check the connection between visible light fluctuations and edge density fluctuation was done at the Caltech tokamak[12] using a 16 channel photodiode array to measure $\tilde{I}$ and a Langmuir probe to measure $\tilde{n}_e$. A high coherence and zero phase difference between $\tilde{I}$ and $\tilde{n}_e$ were found when the two measurements were made within about 1 cm of each other, suggesting that $\tilde{n}_e$ was the dominant cause of $\tilde{I}$. Subsequent Langmuir probe measurements at Caltech[13] and TEXT[14] showed that $\tilde{T}_e/T_e < 0.4\tilde{n}_e/n_e$ in tokamak edge plasmas, suggesting that $\tilde{T}_e$ fluctuations are not dominating $\tilde{I}$. Recent Langmuir probe measurements at ASDEX[15] have also shown $\tilde{n}_e$ edge fluctuations with a structure similar to the earlier ASDEX D_α light emission patterns.

A brief report of the present TFTR visible imaging observations was also given previously in the context of preliminary TFTR edge fluctuation measurements.[16] Subsequent observations of visible light fluctuations from the edge of JET[17] made with unfiltered surface barrier detectors also showed turbulent filaments similar to those in Ref. 16 and the present paper. The JET visible fluctuations had a broadband spectrum with $f < 100$ kHz, a poloidal mode number $m \approx 25$–100, and showed an interesting correlation with the edge $\tilde{B}$ measured with magnetic probes.

IV. TURBULENT FILAMENTS

A. Experimental results

Figure 1 shows some typical examples of the turbulent filamentation of D_α light emission in TFTR. The photos in 1(b)–1(d) are three different video fields each exposed for 15 μsec using the D_α filter during a typical neutral beam injection (NBI) discharge ($I = 1.4$ MA, $P_{\text{beam}} = 12$ MW, $B = 50$ kG, $R = 245$ cm, $a = 80$ cm, discharge #21 819).

The view shown schematically in Fig. 1(a) is from the outer equator toward an area about 100×100 cm along the

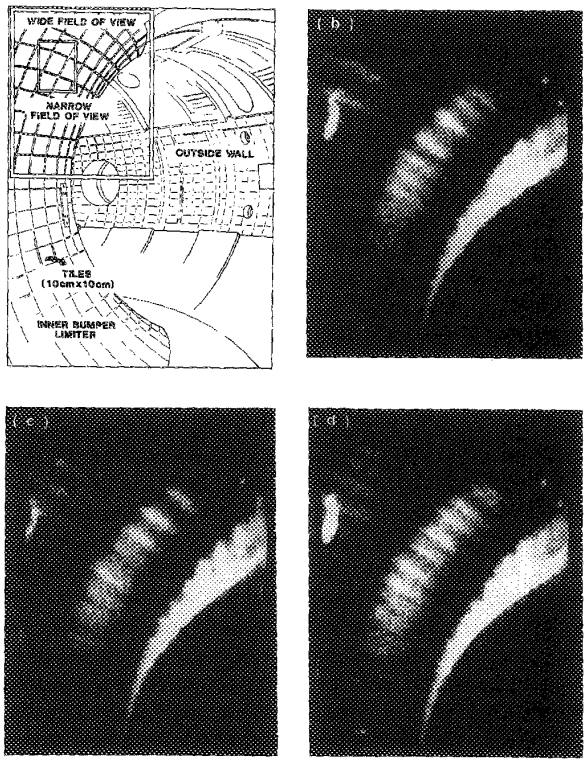

FIG. 1. Images of D_α light emission from the inner wall region of TFTR for a typical neutral-beam-heated plasma. Fig. 1(a) shows the camera's field of view, which for (b)–(d) is the wide field of view. The photos in (b)–(d) are single video fields exposed for 15 μsec taken from a typical TFTR NBI discharge. The D_α light forms toroidally elongated filaments that vary in position randomly from field to field. Note that the toroidal variation of D_α is due to a modulation of the local neutral density. The bright disk at the left is due to enhanced recycling at the edge of a porthole in the inner wall.

inner bumper limiter, which is a toroidally shaped surface made of 10×10 cm carbon tiles. This bumper limiter extends $\pm 60°$ poloidally from the inner midplane and 360° toroidally. The view of Fig. 1 covers a poloidal range 0°–60° above the inner midplane of this limiter and a toroidal angle range of $\approx 45°$ (i.e., about two toroidal field coil periods). Note that all the plasma–wall contact occurs at this bumper limiter, and that none of the neutral beam lines are aimed at this section of the inner wall.

The bright filaments of light seen in Fig. 1 appear to be aligned (approximately) toroidally and are usually irregularly spaced poloidally, as in Figs. 1(b)–(c). Sometimes the poloidal spacing appears to be quite regular, as in Fig. 1(d). The poloidal positions of all of these filaments vary completely from field to field, i.e., none of them remain stationary for 16 msec.

Note that the brightness of these filaments also appears to be varying toriodally; however, this is due to a physical modulation of the inner wall surface itself, which causes the local recycled deuterium neutral density to vary with the toroidal field coil periodicity. Note also that the bright arc of light at the right is the edge of the inner bumper limiter in this view, showing that the D_α light forms an annulus 5–10 cm thick located radially just inside the inner wall.

Figure 2 shows an example of the digitized D_α light intensity as a function of poloidal angle over the range 20°–50° above the inner midplane, taken from a single video field for the discharge of Fig. 1. The fluctuations in light intensity are quite large, often varying by $\pm$ 50% over a poloidal distance of 5–10 cm.

Figure 3 shows several video fields taken with a view similar to that of Fig. 1, but with differing exposure times of (a) 15 μsec, (b) 40 μsec, (c) 160 μsec, and (d) 400 μsec. Each photo is from a different discharge, but all discharges had 10–12 MW of NBI at a plasma current of 0.9 MA and a toroidal field of 50 kG. At exposure times of 15 and 40 μsec the D_α filaments are clearly visible and qualitatively similar to each other, but the filaments are almost completely "blurred" at exposure times of 160 and 400 μsec, suggesting a local autocorrelation time of between 40 and 160 μsec.

Shown in Fig. 4 are several video fields taken using the narrow view indicated in Fig. 1(a), which covers an area about 30×30 cm at a poloidal angle of $\approx 35°$ above the inner midplane. These fields were from a 0.9 MA, 5 MW NBI heated plasma (#24 840) taken with an exposure time of 30 μsec. The local orientation of the filaments with respect to the 3 mm spaces between the 10×10 cm carbon tiles can be seen [the tile edges are exactly poloidal and toroidal, as shown approximately by the white lines in Fig. 4(d)].

From these and similar images the position and orientation of the brightest of these filaments can be adequately defined by eye, as indicated in Fig. 4(d). A distribution of poloidal spacings between adjacent filament maxima is shown in Fig. 5 for two discharges, one at 0.9 MA (#24 840) and another with the same view and exposure time but at 1.4 MA (#24 842), both with 5 MW of NBI. The average poloidal wavelength defined in this way was $\lambda_{pol} \approx 3$ cm for the 0.9 MA case and $\lambda_{pol} \approx 5$ cm for the 1.4 MA case.

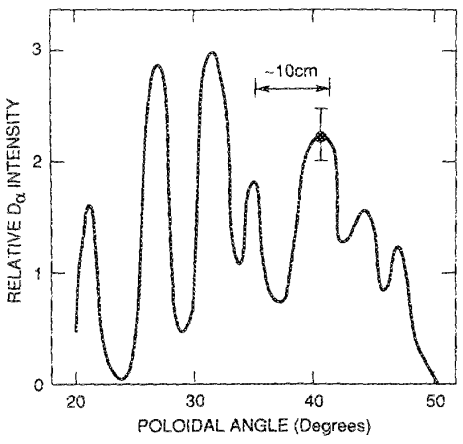

FIG. 2. Digitized D_α light intensity versus poloidal angle from a single video field similar to those in Fig. 1. This intensity is evaluated along a poloidal arc through the bright region near the center of the photos in Fig. 1. The poloidal angle is measured with respect to the inner equator.

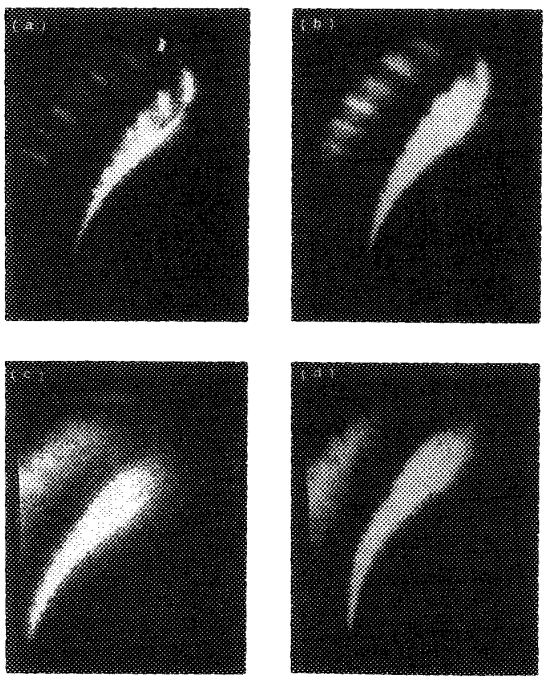

FIG. 3. Variation of the D_α filaments versus camera exposure time. The exposure times are (a) 15 μsec, (b) 40 μsec, (c) 160 μsec, and (d) 400 μsec, taken from similar NBI discharges (#22 871, #22 923, #22 956, and #22 928, respectively). The filament structures are qualitatively similar in (a) and (b) but are blurred out in (c) and (d), indicating a characteristic autocorrelation time of roughly 100 μsec for these fluctuations.

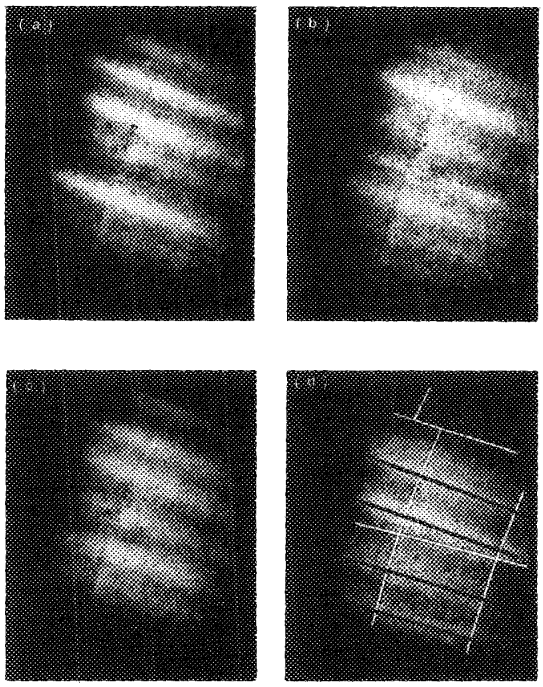

FIG. 4. Images of D_α light from the TFTR inner wall similar to those in Fig. 1 but taken with the narrow field of view shown in Fig. 1(a). In (d) the alignment of the filaments (shown by black lines) can be seen with respect to the toroidal versus poloidal spaces between the 10×10 cm carbon wall tiles (indicated approximately by the white lines). The exposure time was 30 μsec for these fields.

For the same set of filaments the local angle with respect to the toroidal direction was estimated, with results shown in Fig. 6. The average toroidal angle of the filaments was about 4°–5° for the 0.9 MA case and about 6°–7° for the 1.4 MA case, with an uncertainty of about $\pm 2°$ for each filament. The local magnetic field directions (including the poloidal field as calculated from the equilibrium code[18]) are 2° and 3.5°, respectively. Thus the net angle of the filaments with respect to the local magnetic field direction, $\phi_{\rm net}$, combined with the measured poloidal wavelengths of Fig. 5, can be used to estimate a parallel wavelength $\lambda_\parallel$ for these filaments (as measured along the total magnetic field) through $\lambda_\parallel \approx \lambda_{\rm pol}/\phi_{\rm net}$. The average result is $\lambda_\parallel \approx 100$ cm for both cases, but the variation among the filaments and the uncertainty in each measurement are such that $\lambda_\parallel$ ranging from 50 cm to infinity (i.e., $k_\parallel = 0$) are included in this data set.

Several results of a more qualitative nature were also obtained from these images. In general, the D_α light emission at the inner wall during Ohmic plasmas was too dim to see filaments clearly in any single field, although they often seemed (to the eye) to be present when the video tape was replayed at normal speed. When helium gas was used in Ohmic discharges the visible light was brighter (with the D_α filter removed) and filaments did appear clearly, although

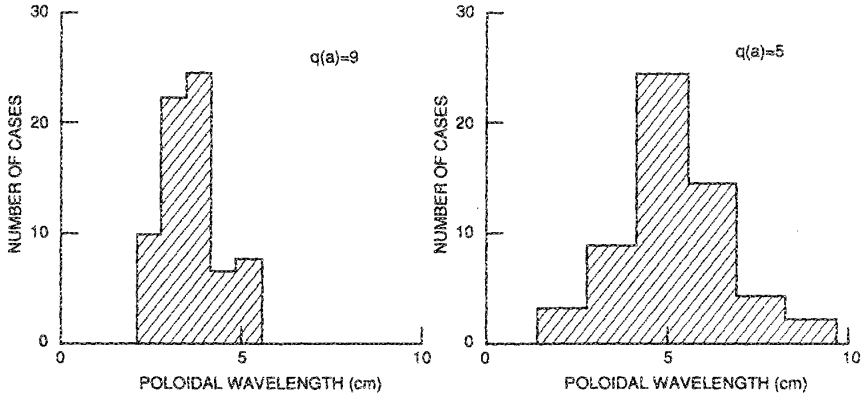

FIG. 5. Poloidal wavelength distribution between adjacent filaments as derived from photos such as those in Fig. 4. The filaments were identified by eye as shown in Fig. 4(d). Results for two different discharges are shown, one at $q(a) \approx 5 (I = 0.9$ MA) and the other at $q(a) \approx 5 (I = 1.4$ MA).

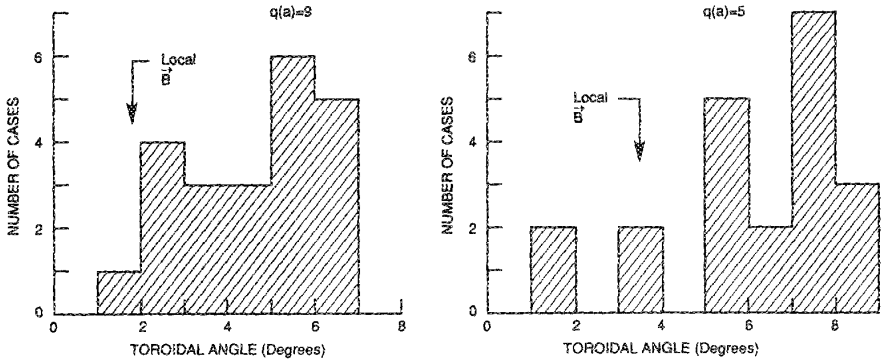

FIG. 6. Toroidal angle distribution of the filaments for the same two discharges as in Fig. 5. The net angle between the filaments and the local magnetic field is about 3°, indicating a relatively small parallel wavelength along the magnetic field for these fluctuations.

not as distinctly as in D_α with NBI. When a carbon III filter at 460 nm (10 nm wide) was used during NBI, dim filaments similar to those seen in D_α were also observed. A videotape showing these features is available from the authors.

A potential application of this technique would be to correlate edge turbulence with changes in plasma parameters. However, at this point we have not attempted such a correlation because qualitatively similar D_α filamentation was seen during *all* NBI discharges in the ranges 0.8–2.2 MA and 5–15 MW during the 1986 TFTR run, including both "L mode" and "supershots." Any quantitative interpretation of some systematic variation of these fluctuations would need to take into account the various possible causes for D_α light variations discussed in Sec. III. For example, a variation in the radial width of the D_α emitting layer resulting from edge profile changes could affect $\tilde{I}/I$ without changes in the local $\tilde{n}_e/n_e$.

B. Tentative interpretations

Several features of these D_α light fluctuations $\tilde{I}$ (where $\tilde{I}$ is integrated over the inner radial shell of D_α) are at least qualitatively similar to edge density fluctuations $\tilde{n}_e$ as previously measured with Langmuir probes in TFTR[16] and smaller tokamaks.[3,14,15] Both $\tilde{n}_e$ and $\tilde{I}$ form toroidally elongated filaments with a poloidal scale much smaller than the plasma minor radius, as in Fig. 1. In addition, both $\tilde{n}_e$ and $\tilde{I}$ are also very large in magnitude in the edge region ($T_e \approx 10$–50 eV), i.e., $\tilde{n}_e/n_e \approx \tilde{I}/I \approx 50\%$, as shown in Fig. 2 for $\tilde{I}$.

These $\tilde{I}$ fluctuations look approximately the same at $\approx 20°$ poloidally above the inner equator to 50° poloidally above the inner equator, where the calculated D_α emission varies from mostly "inside" the last closed flux surface (20°), to mostly within the "scrape-off" region (50°). This is consistent with probe measurements, which show that the edge density fluctuations are approximately unchanged when crossing the last closed flux surface.[3,14] Finally, both $\tilde{n}_e$ and $\tilde{I}$ also have relatively short autocorrelation times, with a typical frequency of ≈ 10 kHz for $\tilde{I}$ (as inferred from Fig. 3) being similar to that measured with probes in the TFTR scrape-off region.[16]

The simplest interpretation of these similarities would be that the $\tilde{I}$ fluctuations are representative of the local $\tilde{n}_e$, i.e., the $\tilde{T}_e$, $\tilde{n}_d$, and radial averaging effects discussed in Sec. III are negligible, at least for those fluctuations in the observable size-scale range $\lambda_{\rm pol} > 2$ cm. Tentatively assuming this, we find several features of the inferred $\tilde{n}_e$ to be new and surprising.

The first new feature is the large fluctuation level at the *inner* major radius where very few edge $\tilde{n}_e$ measurements have been made.[3] This implies that the "good curvature" of this region with respect to MHD interchange instability is not sufficient to stabilize these fluctuations.

The second interesting feature is the poloidal wavelength of these fluctuation. The average poloidal wavelength $\lambda_{\rm pol} \approx 3$–5 cm corresponds to $k_{\rm pol}\rho_S \approx 0.02$ (where $k_{\rm pol} \equiv 2\pi/\lambda_{\rm pol}$ and ρ_s is the ion gyroradius evaluated at the electron temperature) or $m \approx 100$. This is about 10 times *larger* than the $k_\perp \rho_s \approx 0.3$ expected from a collisional drift wave model,[19] but apparently much *smaller* than the $m \approx 10$ expected from a resistive fluid turbulence model.[20] This poloidal wavelength is also much *larger* than expected from an empirical fit to tokamak $\tilde{n}_e$ data given by Surko.[21]

The third new feature is the relatively small parallel wavelength $\lambda_\parallel \approx 100\,{\rm cm} \approx 0.1qR$ cm deduced from the average toroidal angle of the filaments in Fig. 6. This is much smaller than the usual theoretical estimate of a large $\lambda_\parallel \approx qR \approx 1000$–1500 cm set by the high parallel electron conductivity. A similarly short parallel wavelength $\lambda_\parallel \approx 0.1$–$0.3qR$ for edge $\tilde{n}_e$ turbulence has recently been derived from two-probe correlations in TEXT.[22] Note that the TEXT results show (as does Fig. 6) that the filaments tend to be at a larger angle with respect to the toroidal direction than the local magnetic field .

Finally, there is a surprisingly sharply peaked $k_{\rm pol}$ spectrum evident in photos like Fig. 1(d) and in the distributions of Fig. 5, which is in contrast to the usual broad k spectra deduced from probe and scattering measurements.[23,24] This peaking is partly due to the averaging over smaller wavelengths within the D_α emitting region (since $\lambda_{\rm rad} \approx \lambda_{\rm pol}$ for edge $\tilde{n}_e$), and partly due to the finite exposure time (since the smaller wavelengths are presumably "blurred" by the time integration). Nevertheless, there does often appear (to the eye) to be a "quasicoherent" nature to these edge filaments that bears further investigation. Possibly this observation is related to the quasicoherent mode seen near the inner

equatorial plane in scattering measurements in TEXT[25] or during the H mode in PDX.[26]

V. MERFES

A. Experimental results

A second type of edge fluctuation has been observed with this plasma TV imaging system. We call this new phenomenon a "merfe," which suggests its connection to the well-known "marfe."

Marfes ("multifaceted asymmetric radiation from the edge") are poloidally localized, toroidally symmetric edge perturbations that have previously been studied with multichannel imaging systems in Alcator[4] and TFTR.[27] Marfes occur spontaneously in either Ohmic or beam-heated TFTR plasmas near the high-density limit, and are clearly seen in our visible imaging system. Figure 7 shows a typical marfe, which is a solitary toroidal band that starts at the inner equator and moves very slowly poloidally. When the density is raised further, the marfe moves to the top of the vessel and then forms a poloidally symmetric "detached plasma."[28]

Merfes ("moving ensemble of radiations from the edge") are also poloidally localized and toroidally symmetric bands of light, but they have several peculiar features, as shown in Fig. 8. First, several such bands occur simultaneously, as opposed to marfes, which are solitary. A typical merfe pattern first appears clearly during NBI, as shown in Fig. 8(a), when typically five to seven stationary bands are located symmetrically up and down along the inner bumper limiter during NBI. These merfes appear similar when viewed using either all visible light, the D_α line, or the carbon III line, both at very slow (16 msec as in Fig. 8) and very fast ($\approx 40\,\mu$sec) exposure times.

After NBI the visible light emission diminishes due to decreased recycling at the inner wall, but the merfes remain stationary until the plasma current begins to decay. Then at some point during the current decay a remarkable change occurs: the merfes suddenly begin to cascade toward the top (for those previously in the upper half) and bottom (for those previously in the lower half), simultaneously and symmetrically. As old merfes move away from the inner equator, new ones seem to be born there, and these follow the older ones poloidally toward the outer equatorial plane. As this is happening the spacing between merfes at a given poloidal location gradually decreases, until the merfe spacing becomes too small to resolve (≈ 5 cm), and eventually the plasma detaches from the inner wall. The typical merfe behavior as shown in Fig. 8 was observed over the whole range of NBI discharges in 1986 (0.8–2.2 MA, 5–15 MW NBI), but was not always present.

B. Tentative interpretations

The simplest interpretation of these merfe images is that the $\tilde{I}$ fluctuations are due to the local $\tilde{n}_e$ and/or $\tilde{T}_e$, as in Sec. III, which would also be consistent with the usual marfe thermal instability physics.[5] Since the merfes move poloidally beyond the edge of the inner bumper limiter during current decay, it is unlikely that the plasma–wall interaction itself plays an important role in their dynamics.

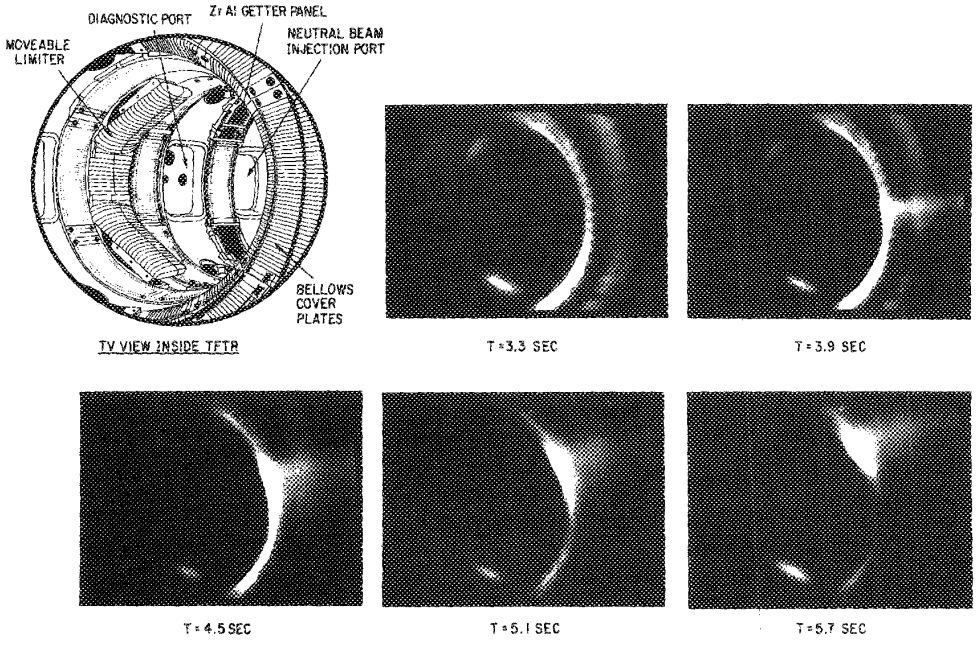

FIG. 7. Example of a marfe in TFTR. The marfe is a bright toroidal band of light which forms at 3.9 sec near the inner equator and slowly moves toward the top of the vessel. This sequence was taken using all visible light at 16 msec exposure time in 1985 when the inner wall was composed of Inconel plates instead of carbon tiles (but similar marfes were observed with carbon walls).

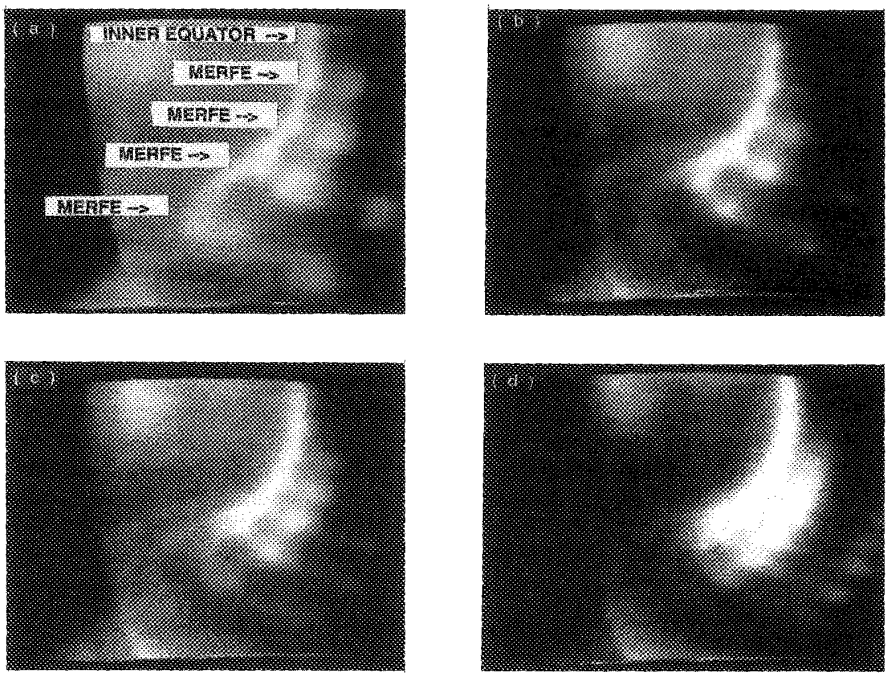

FIG. 8. Example of a merfe in TFTR (discharge #22 029). During NBI the merfe bands are stationary with respect to the inner wall at the positions shown in (a). Note that this is a wide field of view similar to that shown in Fig. 1(a), but of the lower half of the vessel. Just after the plasma current begins to decay (i.e., well after NBI), the merfe bands suddenly begin to move poloidally from the inner midplane toward the outer midplane, as shown in (b)–(d). The merfe structure and movement is symmetrical above and below the midplane.

The merfe's most surprising property is that its poloidal wavelength does *not* correspond to the poloidal mode number $m = q(a)$ set by the magnetic geometry. For example, during steady-state NBI when $q(a) \approx 9$, merfes remain stationary at poloidal angles of approximately $\pm 6°$, $\pm 20°$, and $\pm 36°$ with respect to the inner midplane (see Fig. 8), which corresponds to a poloidal mode number $m \approx 25$. During current decay the average merfe spacing decreases to $m \approx 50$–100 when $q(a) \approx 15$–20. This, along with their toroidally symmetric $n = 0$ structure, implies that merfes are not the same as magnetic "locked modes."

Also surprising about these merfes is their slow (≈ 1 m/sec), smooth poloidal phase velocity both up and down symmetrically away from the inner equator during current decay, which is very different from MHD or local electrostatic mode propagation. Perhaps the merfes are a signature of some internal, radially localized plasma structures that are "peeling off" against the inner wall as the current decays. Such internal structures might be causing previously unexpected edge plasma transport.

VI. CONCLUSIONS

Two types of edge fluctuations were investigated with a visible D_α imaging system viewing the inner wall during high-power NBI in TFTR. The first were seen only with exposure times < 100 μsec and are turbulent "filaments" most likely due to edge density fluctuations. The second are a new phenomenon, "merfes," which are multiple stationary or slowly moving toroidal bands similar to marfes.

These turbulent filaments seen in TFTR with high-power NBI are at least qualitatively similar to those reported in smaller Ohmic tokamaks[2,3,14,15] and also in JET with NBI.[17] However, several interesting new features of these edge fluctuations could be inferred with the present 2-D optical imaging system. For example, the poloidal wavelength of these filaments of ≈ 3–5 cm was much larger than expected from collisional drift wave turbulence models, while their parallel wavelength of ≈ 100 cm was much shorter than expected. There was also (occasionally) a surprisingly coherent structure to these filaments that is not usually associated with edge turbulence, as in Fig. 1(d).

Although these results can be used to clarify the physics of this turbulence, they cannot be used to assess the fluctuation-induced transport directly. However, it seems plausible that this large edge fluctuation level is connected to the unexplained large edge transport in tokamaks.

The "merfe" structure that sometimes appeared during NBI was apparently unrelated to these turbulent filaments, as seen by the peculiar regularity of their poloidal phase velocity after current decay. The merfes are probably similar to marfes, and may indicate a previously unexpected edge transport mechanism during NBI.

Most of these features observed with the optical imaging system in TFTR could not have been observed with conventional fluctuation diagnostics such as Langmuir probes or microwave scattering. However, a difficulty with this optical imaging technique lies in interpreting the spectral line emission. For D_α we argued that the light fluctuations respond mainly to $\tilde{n}_e$, but this was not verified quantitatively. Another difficulty was a lack of time resolution in the video format, but this can be overcome using a set of discrete photomultipliers in parallel with the camera system.

Future application of this method can use a more sensi-

tive camera to examine higher temperature plasma regions, using either the natural impurity line emission (with various narrow-band filters) or the D_α from an injected high-energy neutral hydrogen beam. Such images of the 2-D internal fluctuation pattern could provide some new insight into tokamak turbulence and transport.

ACKNOWLEDGMENTS

We thank M. G. Bell, L. C. Johnson and A. T. Ramsey for help and K. M. Young for support during this project.

This work was performed under U.S. Department of Energy Contract No. DE-AC02-76-CHO3073.

[1]M. G. Bell, V. Arunasalam, C. W. Barnes, M. Bitter, H. -S. Bosch, N. L. Bretz, R. Budny, C. E. Bush, A. Cavallo, T. K. Chu, S. A. Cohen, P. Colestock, S. L. Davis, D. L. Dimock, H. F. Dylla, P. C. Efthimion, A. B. Ehrhardt, R. J. Fonck, E. Fredrickson, H. P. Furth, G. Gammel, R. J. Goldston, G. Greene, B. Grek, L. R. Grisham, G. Hammett, R. J. Hawryluk, H. W. Hendel, K. W. Hill, E. Hinnov, J. Hosea, R. B. Howell, H. Hsuan, R. A. Hulse, K. P. Jaehnig, A. C. Janos, D. Jassby, F. Jobes, D. W. Johnson, L. C. Johnson, R. Kaita, C. Kieras-Phillips, S. J. Kilpatrick, V. A. Krupin, P. H. LaMarche, W. Langer, B. LeBlanc, R. Little, A. I. Lysoyvan, D. M. Manos, D. K. Mansfield, E. Mazzucato, R. T. McCann, M. P. McCarthy, D. C. McCune, K. McGuire, D. H. McNeill, D. M. Meade, S. S. Medley, D. R. Mikkelsen, R. Motley, D. Mueller, J. A. Murphy, Y. Murakami, E. B. Nieschmidt, D. K. Owens, H. Park, A. T. Ramsey, M. H. Redi, A. L. Roquemore, P. H. Rutherford, T. Saito, N. R. Sauthoff, G. Schilling, J. Schivell, G. L. Schmidt, S. D. Scott, J. C. Sinnis, J. Stevens, J. D. Strachan, B. C. Stratton, W. Stodiek, G. D. Tait, G. Taylor, J. R. Timberlake, H. H. Towner, M. Ulrickson, S. von Goeler, R. Wieland, M. Williams, J. R. Wilson, K. -L. Wong, S. Yoshikawa, K. M. Young, M. C. Zarnstorff, and S. J. Zweben, in *Plasma Physics and Controlled Nuclear Fusion Research 1988*, Proceedings of the 12th International Conference, Nice, France (IAEA, Vienna, in press).

[2]D. H. J. Goodall, J. Nucl. Mater. **111/112**, 11 (1982); H. Niedermeyer (private comunication, 1982).

[3]S. J. Zweben and R. W. Gould, Nucl. Fusion **23**, 1625 (1982).

[4]B. Lipschultz, J. Nucl. Mater. **145/147**, 15 (1987).

[5]J. F. Drake, Phys. Fluids **30**, 2429 (1987).

[6]S. S. Medley, D. L. Dimock, S. Hayes, D. Long, J. L. Lowrance, V. Mastrocola, G. Renda, M. Ulrickson, and K. M. Young, Rev. Sci. Instrum. **56**, 1873 (1985).

[7]Camera obtained from Xybion Corp., San Diego, California.

[8]D. H. Heifetz, A. B. Ehrhardt, A. T. Ramsey, H. F. Dylla, R. Budny, D. McNeill, S. Medley, and M. Ulrickson, J. Vac. Sci. Technol. **A6**, 2564 (1988).

[9]L. C. Johnson and E. Hinnov, J. Quant. Spectrosc. Radiat. Transfer **13**, 333 (1973).

[10]D. McNeill, J. Nucl. Mater. **476**, 162 (1989).

[11]L. C. Johnson, Astrophys. J. **174**, 227 (1972).

[12]S. J. Zweben, J. McChesney, and R. W. Gould, Nucl. Fusion **23**, 825 (1983).

[13]P. C. Liewer, J. M. McChesney, S. J. Zweben, and R. W. Gould, Phys. Fluids **29**, 309 (1986).

[14]Ch. P. Ritz, R. V. Bravenec, P. M. Schoch, R. D. Bengtson, J. A. Boedo, J. C. Forster, K. W. Gentle, Y. He, R. L. Hickok, Y. J. Kim, H. Lin, P. E. Phillips, T. L. Rhodes, W. L. Rowan, P. M. Valanju, and A. J. Wootton, Phy. Rev. Lett. **62**, 1844 (1989).

[15]A. Rudyj, R. D. Bengtson, A. Carlson, L. Giannone, M. Krämer, H. Niedermeyer, Ch. P. Ritz, N. Tsois, and the ASDEX Team, in *Proceedings of the 16th European Conference on Controlled Fusion and Plasma Physics*, Venice (E.P.S., Petit-Lancy, Switzerland, in press).

[16]S. J. Zweben, D. Manos, R. Budny, P. Efthimion, E. Fredrickson, H. Greenside, K. Hill, S. Hiroe, S. Kilpatrick, K. McGuire, S. S. Medley, H. Park, A. Ramsey, and J. Wilgen, J. Nucl. Mater. **145-147**, 250 (1987).

[17]M. Malacarne and P. A. Duperrex, Nucl. Fusion **27**, 2113 (1987).

[18]M. G. Bell (private communication).

[19]P. A. Terry and P. H. Diamond, Phys. Fluids **28**, 1419 (1985).

[20]D. R. Thayer, P. H. Diamond, Ch. P. Ritz, H. Biglari, B. A. Carreras, G. G. Craddock, T. S. Hahm, O. J. Kwon, J. K. Lee, N. Ohyabu, P. W. Terry, F. Wagner, A. J. Wootton, and S. J. Zweben, in Ref. 1.

[21]C. M. Surko, Comments Plasma Phys. Controlled Fusion **10**, 265 (1987).

[22]Ch. P. Ritz, E. J. Powers, T. L. Rhodes, R. D. Bengtson, K. W. Gentle, Hong Lin, P. E. Phillips, A. J. Wootton, D. L. Brower, N. C. Luhmann, Jr., W. A. Peebles, P. M. Schoch, and R. L. Hickok, Rev. Sci. Instrum. **59**, 1739 (1988).

[23]S. Crowley and E. Mazzucato, Nucl. Fusion **25**, 507 (1985).

[24]P. C. Liewer, Nucl. Fusion **25**, 543 (1987).

[25]D. L. Brower, W. A. Peebles, and N. C. Luhmann, Jr., Nucl. Fusion **27** 2055 (1987).

[26]R. E. Slusher, C. M. Surko, J. F. Valley, T. Crowley, E. Mazzucato, and K. McGuire, Phys. Rev. Lett. **53**, 667 (1984).

[27]F. P. Boody, C. E. Bush, S. S. Medley, H. K. Park, and J. F. Schivell, J. Nucl. Mater. **145-147**, 196 (1987).

[28]J. D. Strachan, F. P. Boody, C. Bush, B. Grek, R. J. Hawryluk, D. Hiefetz, H. W. Hendel, K. W. Hill, D. W. Johnson, A. T. Ramsey, S. Sesnic, J. F. Schivell, M. Shimada, G. Taylor, and M. C. Zarnstorff, in *Proceedings of the 12th European Conference on Controlled Fusion and Plasma Physics* (E.P.S. Petit-Lancy, Switzerland, 1985), p. 339.